R16, a novel amonafide analogue, induces apoptosis and G_2-M arrest via poisoning topoisomerase II

Hong Zhu,[1] Min Huang,[1] Fan Yang,[1] Yi Chen,[1] Ze-Hong Miao,[1] Xu-Hong Qian,[3] Yu-Fang Xu,[3] Yu-Xin Qin,[1] Hai-Bin Luo,[2] Xu Shen,[2] Mei-Yu Geng,[1,4] Yu-Jun Cai,[1] and Jian Ding[1]

[1]Division of Anti-Tumor Pharmacology, [2]Drug Discovery and Design Center, State Key Laboratory of Drug Research, Shanghai Institute of Materia Medica, Chinese Academy of Sciences; [3]Shanghai Key Laboratory of Chemical Biology, East China University of Science and Technology, Shanghai, P.R. China; and [4]Department of Pharmacology and Glycobiology, Marine Drug and Food Institute, Ocean University of China, Qingdao, P.R. China

Abstract

Amonafide, a naphthalimide derivative, although selected for exploratory clinical trials for its potent anticancer activity, has long been challenged by its unpredictable side effects. In the present study, a novel amonafide analogue, 2-(2-dimethylamino)-6-thia-2-aza-benzo-[*def*]-chrysene-1,3-diones (R16) was synthesized by substituting 5′-NH_2 of the naphthyl with a heterocyclic group to amonafide, with additional introduction of a thiol group. In a panel of various human tumor cell lines, R16 was more cytotoxic than its parent compound amonafide. It was also effective against multidrug-resistant cells. Importantly, the i.p. administration of R16 inhibited tumor growth in mice implanted with S-180 sarcoma and H_{22} hepatoma. The molecular and cellular machinery studies showed that the R16 functions as a topoisomerase II (topo II) poison via binding to the ATPase domain of human topo IIα. The superior cytotoxicity of R16 to amonafide was ascribed to its potent effects on trapping topo II–DNA cleavage complexes. Moreover, using a topo II catalytic inhibitor aclarubicin, ataxia-telangiectasia-mutated (ATM)/ATM- and Rad3-related (ATR) kinase inhibitor caffeine and topo II–deficient HL-60/MX2 cells, we further showed that R16-triggered DNA double-strand breaks, tumor cell cycle arrest, and apoptosis were in a topo II–dependent manner. Taken together, R16 stood out by its improved anticancer activity, appreciable anti–multidrug resistance activities, and well-defined topo II poisoning mechanisms, as comparable with the parent compound amonafide. All these collectively promise the potential value of R16 as an anticancer drug candidate, which deserves further development. [Mol Cancer Ther 2007;6(2):484–95]

Received 9/19/06; revised 11/2/06; accepted 12/28/06.

Grant support: National Natural Science Foundation of China grant 30572201.

The costs of publication of this article were defrayed in part by the payment of page charges. This article must therefore be hereby marked *advertisement* in accordance with 18 U.S.C. Section 1734 solely to indicate this fact.

Requests for reprints: Jian Ding, Division of Anti-Tumor Pharmacology, State Key Laboratory of Drug Research, Shanghai Institute of Materia Medica, Chinese Academy of Sciences, 555 Zu Chong Zhi Road, Zhangjiang Hi-Tech Park, Shanghai 201203, P.R. China. Fax: 86-21-50806722. E-mail: jding@mail.shcnc.ac.cn

doi:10.1158/1535-7163.MCT-06-0584

Introduction

DNA topoisomerase II (topo II) is a nuclear enzyme that solves topological problems of DNA in replication, transcription, recombination, and chromosome condensation and decondensation via a DNA breakage/reunion mechanism (1). A wide range of topo II–targeted inhibitors are commonly classified as topo II poisons and catalytic inhibitors (2–4). In fact, all the topo II–targeted anticancer drugs clinically used for their antitumor activities belong to topo II poisons, which have been commonly recognized to interrupt the breakage/reunion reaction of the enzyme, resulting in the accumulation of topo II–DNA covalent intermediate, the cleavage complex, and causing cancer cell death (2). However, the most widely used topo II poisons, including etoposide, Adriamycin, and their analogues, often induce dose-limiting toxicities and multidrug resistance (MDR), resulting in treatment failure after initial effective therapy. As such, increasing research is focused on the development of novel topo II–targeted drugs, with the aim of overcoming current restrictions.

Naphthalimides were designed by combining structural components of several antitumor compounds into a small molecule (5). One of these compounds, amonafide (National Service Center 308847; Fig. 1), was selected for exploratory clinical development by the National Cancer Institute and showed activity in breast cancer (6, 7). It has been verified to exert topo II–mediated DNA cleavage in a cell-free system (8). Clinical studies found that amonafide was extensively metabolized to *N*-acetyl-amonafide via *N*-acetylation by *N*-acetyltransferase 2. This metabolite caused a high-variable, unpredictable toxicity because of the interindividual differences in *N*-acetylation and greatly obstructed its clinical development (9, 10). Challenged by such a toxic issue, some groups took efforts to develop the individualized dosing regimen of amonafide based on pharmacodynamic profiles, with particular incorporation of acetylator phenotype and gender (11, 12). Others resorted to the combined chemotherapy of amonafide with 1-β-D-arabinofuranosylcytosine, producing efficacy for patients with poor-risk acute myelogenous leukemia (13). More appreciable naphthalimide derivatives with favorable pharmacologic profiles have been encouraged to be designed and synthesized (14, 15).

2-(2-Dimethylamino)-6-thia-2-aza-benzo-[*def*]-chrysene-1,3-diones (R16) is a novel thio-heterocyclo-naphthalimide

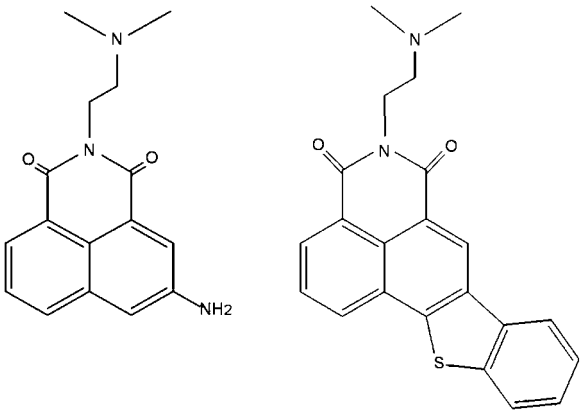

Amonafide R16

Figure 1. Chemical structure of R16 and amonafide.

(Fig. 1; ref. 16). One of the major strategies in this regard has been to improve the intercalation and photocleavage to DNA by chemical modification. It is manipulated by substituting the 5′-NH_2 of the naphthyl of a heterocycle to amonafide for avoiding the release of *N*-acetylated metabolites, with the additional introduction of a thiol group to enhance cytotoxicity via facilitating the interaction of naphthyl heterocycles with DNA (17).

Except for the preliminary illustration of the amonafide as a topo II inhibitor in a cell-free system, little effort has been made to elucidate the detailed contribution of the naphthalimides in this regard. In the present study, we initially evaluated the antitumor efficiency of R16 both *in vitro* and *in vivo* with amonafide in comparison. In addition, we verified the intrinsic inhibitory profiles of R16 on topo II, aiming to figure out the distinct involvement of R16 in particular, and naphthalimides in general, in targeting topo II and its subsequent events.

Materials and Methods

Reagents

R16 was synthesized as previous reported (16), and its purity was more than 99%. Amonafide was obtained from the Drug Synthesis and Chemistry Branch, Division of Cancer Treatment, National Cancer Institute (Berthda, MA). Etoposide (VP16), Adriamycin (ADR), mitoxantrone (MIT), camptothecin (CPT), aclarubicin, and caffeine were purchased from Sigma (St. Louis, MO). All these compounds except caffeine were dissolved in DMSO as stock solutions. Caffeine was dissolved in sterilized water. The stock solutions were kept frozen in aliquot at −20°C and thawed immediately before each experiment.

Cell Lines and Cell Culture

Human gastric adenocarcinoma cell line SGC-7901, hepatocellular carcinoma BEL-7402, cervical carcinoma HeLa, and ovarian epitheloid carcinoma HO-8910 were obtained from the cell bank of the Shanghai Institute of Materia Medica, Chinese Academy of Sciences. Human lung adenocarcinoma cell line A549 was from the National Cancer Institute. Human hepatocellular carcinoma SMMC-7721 was a gift from the Second Military Medical School. Human premyelocytic leukemia HL-60 and the mitoxantrone-resistant variant HL-60/MX2, chronic myelogenous leukemia K562, hepatocellular carcinoma Hep-G_2, oral squamous cell carcinoma KB, colorectal carcinoma HCT-15 and HT-29, and breast carcinoma MDA-MB-468 were purchased from the American Type Culture Collection (Manassas, VA). Human gastric adenocarcinoma MKN-45, colorectal carcinoma HCT-116, breast carcinoma MCF-7, MDA-MB-435, and ovarian carcinoma OVCAR-5, SK-OV-3 were from the Japanese Foundation of Cancer Research (Tokyo, Japan). Rhabdomyosarcoma Rh-30 cell line was a gift from the St. Jude Children's Research Hospital (Memphis, TN). Both Adriamycin-selected MDR cell subline K562/A02 and MCF-7/ADR were purchased from the Institute of Hematology, Chinese Academy of Medical Sciences (Tianjin, China). The vincristine (VCR)-selected MDR KB/VCR subline was obtained from the Zhongshan University of Medical Sciences (Guangzhou, China). All these cell lines except MCF-7 were maintained in RPMI 1640 (Life Technologies, Grand Island, NE) supplemented with 10% heat-inactivated fetal bovine serum (Life Technologies), L-glutamine (2 mmol/L), penicillin (100 IU/mL), streptomycin (100 μg/mL), and HEPES (10 mmol/L; MCF-7 with additional 1 mmol/L sodium pyruvate and supplemented with 0.01 mg/mL bovine insulin; pH 7.4) in a humidified atmosphere of 95% air plus 5% CO_2 at 37°C.

Cell Proliferation Assay

Cell proliferation was evaluated by sulforhodamine B protein staining assay (18). Briefly, cells were seeded into 96-well plates and cultured overnight, treated with R16 or amonafide for 72 h. Cells were then fixed with 10% trichloroacetic acid and stained with sulforhodamine B (Sigma). Sulforhodamine B in the cells was dissolved in 10 mmol/L Tris-HCl and was measured at 515 nm using a multiwell spectrophotometer (VERSAmax, Molecular Devices, Sunnyvale, CA). The inhibition rate on cell proliferation was calculated for each well as $(A515_{control\ cells} - A515_{treated\ cells})/A515_{control\ cells} \times 100\%$ (A515: OD value at 515 nm). The average IC_{50} values were determined by Logit method from at least three independent tests. The resistance factor (RF) was calculated as the ratio of IC_{50} value of the compound in resistant cells to that of parental cells (19).

Propidium Iodide Staining for Flow Cytometry

HL-60 cells (5×10^5/mL) were seeded into six-well plates and exposed to R16 or amonafide for indicated times. Cells were then harvested and washed with PBS, fixed with precooled 70% ethanol at 4°C. Staining went along in PBS containing 40 μg/mL RNase A and 10 μg/mL propidium iodide (Sigma) in the dark for 30 min. For each sample, at least 1×10^4 cells should be analyzed using an FACS-Calibur cytometer (Becton Dickinson, San Jose, CA).

DNA Agarose Gel Electrophoresis

HL-60 cells in six-well plates (5×10^5/mL) were exposed to R16 or amonafide for 24 h. DNA fragmentation was

extracted as in a previous report (20). Briefly, harvested cells were lysed by equal volumes of 1.2% SDS. By adding 7/10 volume of the precipitation solution (3 mol/L CsCl, 1 mol/L potassium acetate, 0.67 mol/L acetic acid) and spinning for 15 min at 14,000 × *g*, DNA fragmentation was kept in the supernatant, which was then absorbed by a miniprep spin column. Finally, DNA was eluted with 50 μL TE buffer (pH, 8.0) and electrophoresed in parallel on the same 1.5% agarose gel in 1× TAE buffer with 0.5 mg/mL ethidium bromide staining to facilitate visualization by fluorescence under UV light. Molecular weight standards (GeneRuler 100 bp DNA Ladder Plus; Fermentas, Burlington, Canada) were run on the left-hand lane of the same gel. Images were captured using Genesnap 6.00.26 software (Syngene, Cambridge, England).

Terminal Deoxynucleotidyl Transferase–Mediated Nick End Labeling Assay

Terminal deoxynucleotidyl transferase–mediated nick end labeling (TUNEL) assay was done according to the manufacturer's instructions (Roche, Basel, Switzerland). Briefly, HL-60 cells (5×10^5/mL) were incubated for 24 h with R16 or amonafide and stained for TUNEL. Cells were washed in PBS twice, fixed in 4% paraformaldehyde, and permeabilized in 0.1% Triton X-100 on ice. For the labeling reaction, the cells were stained for 1 h at 37°C. Samples washed with PBS were observed in a fluorescent microscope (Olympus BX51, Tokyo, Japan).

Neutral Single-Cell Gel Electrophoresis Assay

HL-60 cells (5×10^5/mL) were treated with either R16 or amonafide for 1 h. DNA double-strand breaks (DSB) were evaluated by neutral single-cell gel electrophoresis assay, which was done according to the method developed by Singh (21) with slight modifications (22). A fluorescence microscope (Olympus BX51) was used to capture the images. To describe and evaluate the damage, the olive tail moment (arbitrary units, defined as the product of the percentage of DNA in the tail multiplied by the tail length) analyzed by Komet 5.5F (Kinetic Imaging Ltd., Nottingham, United Kingdom) was used.

kDNA Decatenation Assay

Topo II activity was measured by the ATP-dependent decatenation of kinetoplast DNA (kDNA) (23). The kDNA decatenation assay reaction buffer consisting of 50 mmol/L Tris-HCl (pH 7.7), 120 mmol/L KCl, 10 mmol/L $MgCl_2$, 1 mmol/L ATP, 0.5 mmol/L DTT, 0.5 mmol/L EDTA, and 30 μg/mL bovine serum albumin was mixed with 0.1 μg kDNA, 1 unit of human topo IIα (Topogen, Columbus, OH) and the indicated concentrations of compounds in a total volume of 15 μL. After incubation at 37°C for 15 min, the reaction was terminated by the addition of 10% SDS (1 μL). The DNA samples were subjected to electrophoresis in a 1% agarose gel in 1× TAE at 4 V/cm for 2 h.

Trapped in Agarose DNA Immunostaining Assay

Trapped in agarose DNA immunostaining (TARDIS) assay was done as previously reported (22, 24). Briefly, untreated or treated cells were harvested and mixed with low-melting gel spreading on slides, followed by placing the slides in lysis buffer containing protease inhibitors. Proteins that were not covalently bound to the DNA were then removed by 1 mol/L NaCl containing protease inhibitors. Topo II that covalently bound to DNA of each cells was detected using topo IIα–specific polyclonal antibody (Santa Cruz Biotechnology, Santa Cruz, CA) and Alexa Fluor 488 goat anti-rabbit immunoglobulin G (Molecular Probes, Eugene, OR). DNA was stained with 4′,6-diamidino-2-phenylindole (1 μg/μL). Images were captured using fluorescence microscope (Olympus BX51).

Surface Plasmon Resonance Spectroscopy

Human topo IIα ATPase domain were purified by Chaoxin (25) using the expression vectors for human topo IIα ATPase domain and the yeast BCY123, which were provided by Prof. Tao-shih Hsieh (Department of Biochemistry, Duke University Medical Center, Durham, NC) as previously reported (26). The binding of compounds to human topo IIα ATPase domain was determined by surface plasmon resonance in a BIAcore 3000 instrument (Biacore AB, Uppsala, Sweden) equipped with a human topo IIα ATPase domain immobilized CM5 sensor chip at 25°C as described previously (25). Compound solutions at various concentrations were prepared in HBS-EP buffer. The final compound solutions contained 1% DMSO. Each injection of solution was carried out from the lowest to the highest concentration, and sensorgrams were recorded. The data were analyzed by the evaluation software Build-in BIAeval 3.2. Each data point obtained at the end of the association time was plotted against the concentration and analyzed using the Sigma plot to give the equilibrium dissociation constant (K_D) for each compound.

Preparation of Total Cell Extracts and Immunoblots Analysis

HL-60 cells (5×10^5/mL) were treated with compounds for indicated times. Cells were harvested and resuspended in lysis buffer (50 mmol/L Tris-HCl, 150 mmol/L NaCl, 1 mmol/L EDTA, 0.1% SDS, 0.5% deoxycholic acid, 0.02% sodium azide, 1% NP40, 2.0 μg/mL aprotinin, 1 mmol/L phenylmethylsulfonyl fluoride). The lysates were centrifuged at 10,000 × *g* for 15 min at 4°C. Equivalent amounts of proteins were analyzed by SDS-PAGE. Appropriate antibodies to anti–caspase-3, anti–poly-ADP-ribose polymerase (PARP), anti-Bid, anti-Bax, and anti–β-actin from Santa Cruz Biotechnology; and anti–caspase-8, anti–caspase-9, anti–cleaved-caspase-3, anti–Bcl-xL, anti–Bcl-2, and anti–γ-H_2Ax from Cell Signaling Technology (Beverly, MA) were used. Proteins were visualized with peroxidase-coupled secondary antibody from Southern Biotech (Birmingham, United Kingdom), using ECL-plus kit from Amersham Biosciences (Buckinghamshire, United Kingdom) for detection.

Preparation of Cytosol Fraction and Release of Cytochrome *c*

HL-60 cells (5×10^5/mL) were exposed to R16 or amonafide for 24 h. The separation of mitochondria and cytosol was accomplished as described previously (27) with slight modifications (28). Briefly, cells were harvested, resuspended in an extraction buffer [20 mmol/L HEPES (pH 7.5), 1.5 mmol/L $MgCl_2$, 10 mmol/L KCl, 1 mmol/L

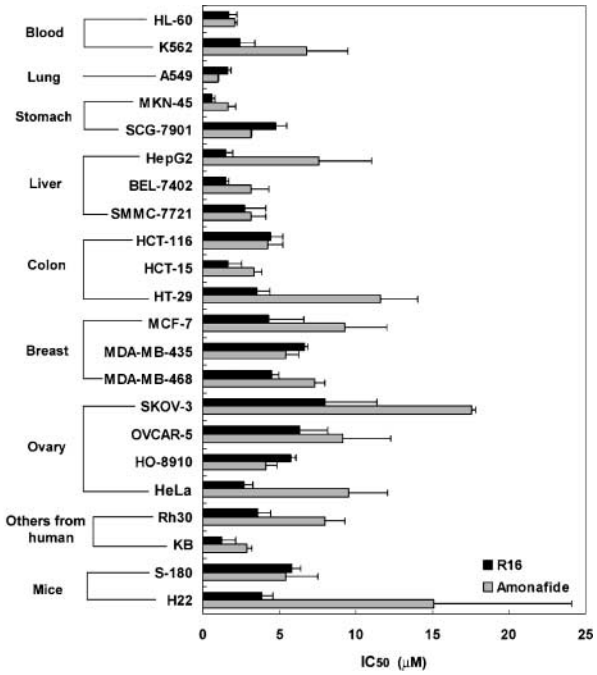

Figure 2. Cytotoxicity of R16 and amonafide against different kinds of tumor cell lines and MDR cell lines. Three separate experiments were carried out to determine the values of IC_{50}, expressed as mean ± SD (μmol/L), and the inhibition rates of each concentration of compounds were tested in triplicate.

EDTA, 1 mmol/L EGTA, 1 mmol/L DTT, 0.1 mmol/L phenylmethylsulfonyl fluoride, and 250 mmol/L sucrose], and homogenized using a microhomogenizer. The homogenates were centrifuged at 750 × *g* for 10 min at 4°C. The supernatants were centrifuged at 10,000 × *g* for 15 min at 4°C, and the remaining supernatant was designated as the cytosol fraction. After Western blot analysis, anti–cytochrome *c* antibodies (Cell Signaling Technology) and anti–apoptosis-inducing factor (AIF) antibodies (Santa Cruz Biotechnology) were used to evaluate the mitochondrial release of cytochrome *c* and AIF.

Animals and Antitumor Activity *In vivo*

Seven-week-old specific pathogen-free female Kunming mice (weight, 18–22 g) were supplied by the Shanghai Laboratory Animal Center, Chinese Academy of Sciences. Mice were inoculated s.c. into the right armpit with S-180 sarcoma or H_{22} hepatoma cells. After 24 h, 5-fluorouracil or normal saline was administered by i.v. injection for 7 days, and R16 or amonafide at indicated doses was administered by i.p. injection for the indicated days. After treatment, animals were killed by cervical dissociation, and solid tumors were removed and weighed. The inhibition rate was calculated as [(average tumor weight of normal saline group − average tumor weight of test group)/average tumor weight of normal saline group] × 100%.

Statistical Analysis

Data were presented as mean ± SD, and significance was assessed with the Student's *t* test. Differences were considered significant at $P < 0.05$.

Results

R16 Inhibits Cancer Cell Proliferation *In vitro*

R16 Is Highly Cytotoxic to Various Tumor Cell Lines. We first determined the effects of R16 on the growth of the human cancer cell lines and mouse tumor cells. R16 displayed potent cytotoxicity in a dose-dependent manner in diversified cancer cell lines, including leukemia, lung cancer, gastric cancer, hepatocellular cancer, colon cancer, breast cancer, ovarian cancer, cervical cancer, rhabdomyosarcoma, and oral epidermoid cancer cell lines, without exhibiting distinct specificity (Fig. 2). The average IC_{50} values of R16 and amonafide against the 20 human tumor cell lines tested were 3.47 and 6.05 μmol/L, respectively. R16 seemed to be more potent than amonafide against leukemia and some solid tumors cells, such as liver cancer, colon cancer, and ovary cancer, with the IC_{50} values of 2.08, 1.92, 3.22, and 5.67 μmol/L, respectively, all below the responding values of amonafide (4.45, 4.63, 6.41, and 10.10 μmol/L, respectively). As for mouse tumor cells, R16 exhibited equivalent growth inhibition on S-180 cells, but displayed more a potent effect on H_{22} cells (Fig. 2).

Table 1. Effects of R16 and amonafide on the MDR sublines

Compounds	IC_{50} (mean ± SD) (μM)		RF	IC_{50} (mean ± SD) (μM)		RF	IC_{50} (mean ± SD) (μM)		RF
	K_562	K_562/A02		KB	KB/VCR		MCF_7	MCF_7/ADR	
R16	2.43 ± 0.94	2.07 ± 0.35	0.85	1.25 ± 0.90	3.31 ± 0.41*	2.64	4.30 ± 2.29	6.07 ± 1.61	1.41
Am	6.81 ± 2.65	6.34 ± 0.38	0.93	2.86 ± 0.34	8.46 ± 0.73†	2.96	9.24 ± 2.77	9.24 ± 3.41	1.00
VP16	5.12 ± 0.94	258.81 ± 84.52†	50.59	0.45 ± 0.08	163.05 ± 76.93†	300.99	15.44 ± 5.16	487.41 ± 40.23*	31.57
ADR	0.40 ± 0.19	46.57 ± 11.42†	117.01	NT	NT	NT	1.55 ± 0.77	150.30 ± 68.65*	96.86
VCR	NT	NT	NT	3.11 ± 1.56‡	0.61 ± 0.03†	197.39	NT	NT	NT

NOTE: Three separate experiments were carried out to determine the values of IC_{50}, expressed as mean ± SD (μmol/L), and the inhibition rates of each concentration of compounds were tested in triplicate. The resistance factor was calculated as the ratio of the IC_{50} value of the MDR cells to that of the corresponding senaltive parental cells. The significance of IC_{50} values of each compound against MDR cells and corresponding parental cells was analyzed and indicated.

* $P < 0.05$.

† $P < 0.01$.

‡ The IC_{50} of VCR against KB cells was 3.11 ± 1.56 nmol/L.

Table 2. Effects of R16 on the growth of S-180 sarcoma and H_{22} hepatoma in mice

Tumor	Treatment group	Dosage (mg × kg^{-1} × d^{-1}) × d	Mice number (initial/end)	Body weight (g) (initial/end)	Tumor weight (g)	Inhibition rate (%)	*t* test*
S-180	NS	–	20/20	19.7/35.2	1.99 ± 0.56	–	
	R16	30 × 6 (i.p.)	10/10	19.5/18.4	0.49 ± 0.25	75.4	$P < 0.01$
	R16	15 × 7 (i.p.)	10/10	19.7/27.9	1.17 ± 0.34	41.2	$P < 0.01$
	R16	7.5 × 7 (i.p.)	10/10	19.9/31.1	1.91 ± 0.44	4.0	$P > 0.05$
	Amonafide	30 × 7 (i.p.)	10/10	19.7/19.0	0.45 ± 0.28	77.4	$P < 0.01$
	5-FU	50 × 2 (i.v.)	10/10	19.4/30.0	0.61 ± 0.24	69.3	$P < 0.01$
H_{22}	NS	–	20/20	20.7/33.6	1.57 ± 0.41	–	
	R16	30 × 5 (i.p.)	8/8	20.9/19.6	0.43 ± 0.14	72.6	$P < 0.01$
	R16	15 × 7 (i.p.)	8/8	21.0/24.0	0.77 ± 0.31	51.0	$P < 0.01$
	Amonafide	30 × 7 (i.p.)	8/8	20.8/24.8	1.34 ± 0.46	14.6	$P > 0.05$
	5-FU	75 × 2 (i.v.)	10/10	20.7/24.7	0.14 ± 0.07	91.1	$P < 0.01$

Abbreviations: NS, normal saline; 5-FU, 5-fluorouracil.
*The Student's *t* test was used to assess the significance of tumor growth inhibition of each group compared with normal saline–treated group.

R16 Highlights its Potency in MDR Cell Lines. MDR is an intractable obstacle of conventional chemotherapeutic drugs in treating human cancers. We examined the cytotoxicity of R16 and amonafide and reference compounds (Adriamycin, vincristine, and VP16) in three MDR-expressing sublines: K562/A02, MCF-7/ADR, and KB/VCR (Table 1). For each of these cell lines, we calculated the RF as the ratio of the IC_{50} value of resistant cells to that of the parental cells. R16 and amonafide displayed approximately equivalent cytotoxicity against the three MDR cell

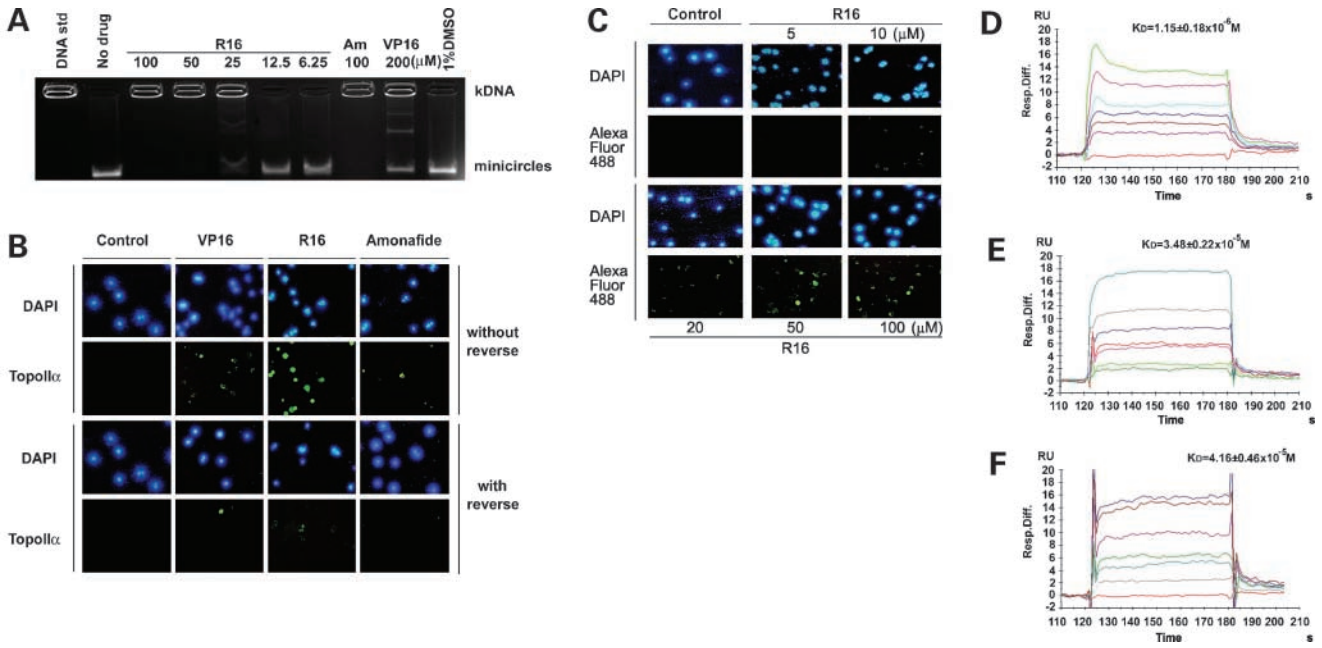

Figure 3. R16 and amonafide were topo II poisons. **A,** R16 or amonafide inhibited topo II–mediated kDNA decatenation in the cell-free system. The following control samples were shown: kDNA (*DNA std*) and minicircles (*No drug*). The positions of kDNA and minicircles were indicated. **B,** R16 and amonafide trapped DNA–topo II complexes in HL-60 cells detected by the TARDIS assay. HL-60 cells were untreated or treated with VP16 (50 μmol/L) or R16 (50 μmol/L) or amonafide (100 μmol/L) for 2 h. Rows *1* and *3*, 4′,6-diamidino-2-phenylindole (*DAPI*)–stained DNA; *rows 2* and *4*, fluorescein-stained topo IIα. *Rows 1* and *2*, samples without incubation in 55°C before lysis; *rows 3* and *4*, samples incubated in 55°C before lysis. Representative images were shown (200×). **C,** the formation of R16-induced topo II cleavage complexes was dose dependent. HL-60 cells were exposed to R16 (0, 5, 10, 25, 50, and 100 μmol/L) for 1 h, and the cleavage complexes were detected using TARDIS assays. **D–F,** interaction of R16 (**D**), amonafide (**E**), and VP16 (**F**) with immobilized human topo IIα ATPase domain measured by surface plasmon resonance spectroscopy. R16 was injected at the concentrations of 0, 0.3125, 0.625, 1.25, 2.5, 5, and 10 μmol/L (*from bottom to top*); amonafide and VP16 were injected at the concentrations of 0, 3.125, 6.25, 12.5, 25, 50, and 100 μmol/L (*from bottom to top*). Sensorgram responses at equilibrium were plotted against each concentration of compounds and the equilibrium dissociation constant (K_D) of the binding system was yielded. The value for the K_D of the binding systems was 1.15, 34.8, and 41.6 μmol/L for R16, amonafide, and VP16, respectively.

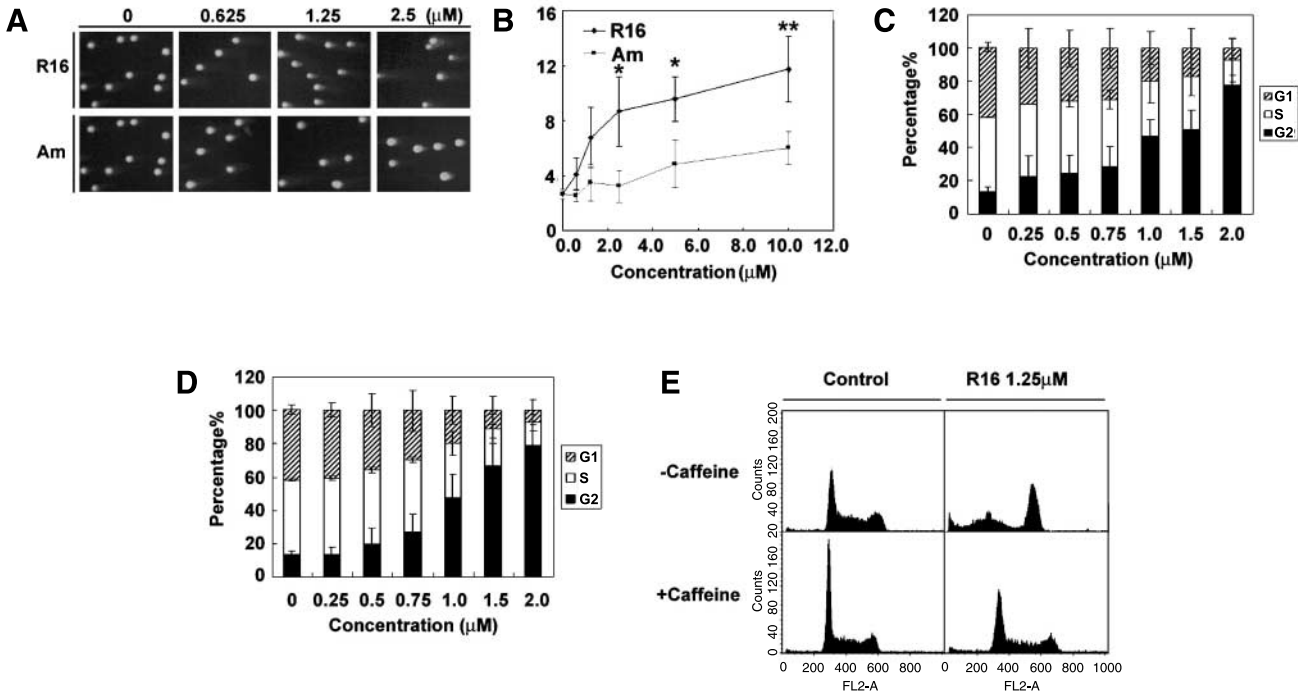

Figure 4. R16-induced, DNA DSB-mediated G_2-M arrest in HL-60 cells. **A,** R16- and amonafide-induced DSBs in HL-60 cells. Cells were untreated or treated with serial diluted concentration of R16 or amonafide for 1 h. Detection of DSBs was done using the neutral comet assay. Representative comet images were shown (200×). **B,** semiquantitative analysis of the results presented in **A**, expressed as the olive tail moment (mean ± SD, $n = 3$). The significance of the data was analyzed and indicated. *, $P < 0.05$; **, $P < 0.01$. **C,** cell cycle distribution histogram of HL-60 cells treated with R16 from the concentration of 0.25 to 2 μmol/L for 24 h representative of three independent experiments. **D,** HL-60 cell cycle distribution treated with amonafide from the concentration of 0.25 to 2 μmol/L. **E,** ATM/ATR inhibitor caffeine (2 mmol/L) abrogated R16-induced G_2-M arrest. *Top*, samples without preincubation of caffeine; *bottom*, samples with preincubation of caffeine.

lines with average RF values of 1.63 and 1.63, which were much lower than those of reference drugs VP16, Adriamycin, and vincristine (147.72, 106.94, and 197.39).

R16 Arrests Tumor Growth in Mice Implanted with S-180 Sarcoma and H22 Hepatoma

Kunming female mice inoculated with S-180 sarcoma cells and H_{22} hepatoma were used to evaluate the effect of R16 on tumor growth *in vivo*. R16 produced dose-dependent effects in mice S-180 sarcoma and H_{22} hepatoma models (Table 2). In S-180 sarcoma models, the i.p. administration of R16 at a dose of 15 mg/kg for 7 days reduced 41.2% tumor growth and, at 30 mg/kg for 6 days, reduced 75.4% tumor growth. In H_{22} hepatoma models, the i.p. administration of R16 at a dose of 15 mg/kg for 7 days reduced 51.0% tumor growth and, at a dose of 30 mg/kg for 5 days (from the first to the fifth day), reduced 72.6% tumor growth. Amonafide at a dose of 30 mg/kg with the same schedule gave an equivalent inhibition effect (77.4%) with R16 in S-180 sarcoma models, but caused much less potent reduction in tumor growth (14.6%) in H_{22} hepatoma models.

R16 Poisons Topo II via Binding to ATPase Domain

Limited reports revealed that the naphthalimides, including amonafide, is likely to target topo II (8). In this context, several experiments were collectively applied to confirm the effect of R16 on topo II at both molecular and cellular levels in the present studies.

R16 Inhibits the Catalytic Activity of Topo II in a Cell-Free System. The kDNA decatenation assay was first done to test whether R16 could inhibit the catalytic activity of topo II. Topo II catalyzed the double-stranded catenated kDNA decatenation in the presence of ATP. Inhibition of topo IIα activity by R16 was measured as a loss in the capacity to decatenate kDNA. As shown in Fig. 3A, in the absence of compounds, kDNA was decatenated to minicircles, which disappeared in a dose-dependent manner in the presence of VP16, R16, or amonafide, and 25 μmol/L R16 was sufficient to inhibit the activity of topo IIα in a cell-free system.

R16 Induces Stable DNA–topo II Complexes. Next, the TARDIS assay was used to detect the formation of topo II–DNA cleavage complexes at the cellular level (22, 24). Heat-induced reversibility is a unique property of topo II cleavage complexes (29). Figure 3B shows typical images of those observed after staining with topo IIα antibody and the Alexa Flour 488 probe. Rows 1 and 3 show DNA-specific blue 4′,6-diamidino-2-phenylindole-staining of cells. No or few visible green immunofluorescence associated with DNA was seen in untreated cells or those that were secondly incubated at 55°C for 10 min after harvesting, respectively. Those treated with VP16 at 50 μmol/L or amonafide at 100 μmol/L seemed to have detectable immunofluorescence, whereas the R16-treated sample (50 μmol/L) released much higher levels of

immunofluorescence. This finding showed that R16 was more potent in trapping reversible topo II cleavage complexes than VP16 and amonafide, promising R16 a favorable topo II poison at the cellular level. Additionally, R16 at 10 μmol/L was sufficient to trap cleavage complexes within 1 h (Fig. 3C).

R16 Binds to the ATP Domain of Human Topo IIα. We next determine whether the above-mentioned inhibition effect of R16 is associated with its direct binding to topo IIα. For this, we measured the binding of R16 to the ATPase domain of human topo IIα using surface plasmon resonance. Recombinant human topo II ATPase domain purified from yeast was immobilized on CM-5 sensor chips. The response binding unit of R16 to the ATPase domain was recorded. Results indicated that R16 revealed a relative high-binding affinity for the ATPase domain, yielding the equilibrium dissociation constant (K_D) of 1.15 μmol/L (Fig. 3D), which was much higher than that of amonafide (34.8 μmol/L; Fig. 3E) and VP16 (41.6 μmol/L; Fig. 3F).

R16 Induces DNA DSBs

Agents capable of trapping topo II–DNA complexes might result in DNA DSBs. We then tested whether R16 triggered the DNA DSBs. Using the neutral single-cell gel electrophoresis, a simple method for measuring DNA DSBs in eukaryotic cells, we found that the exposure of HL-60 cells to R16 within 1 h induced much more DNA DSBs than that of amonafide (Fig. 4A), which was quantified with the software Komet 5.5 (Fig. 4B).

R16 Induces DSBs-Mediated G_2-M Arrest at Low Doses

R16 Induces G_2-M Arrest in HL-60 Cells at Low Doses. Topo II poisons often induce cell cycle arrest, probably because of the generation of DNA DSBs. In the current study, R16 and amonafide induced G_2-M arrest in a dose-dependent manner (Fig. 4C and D). Most of the cells have arrested in the G_2-M phase in HL-60 cells after 24 h treatment (77.64% for 2 μmol/L R16 and 79.19% for 2 μmol/L amonafide).

Caffeine Antagonizes R16-Induced G_2-M Arrest. Ataxia-telangiectasia-mutated (ATM) and ATM- and Rad3-related (ATR) kinases are two phosphatidylinositol 3-kinase–related kinase family of kinases playing important roles in the DNA damage response. Caffeine, an ATM/ATR kinase inhibitor (30), was used to clarify the role of ATM and/or ATR in the R16-induced G_2-M arrest in HL-60 cells. As shown in Fig. 4E, preincubation with 2 mmol/L caffeine for 30 min markedly abrogated R16-induced G_2-M arrest, suggesting the G_2-M arrest was caused by DNA DSBs, which were sensed by ATM and/or ATR.

R16 Triggers DNA DSB-Mediated Apoptosis

R16 Induces Apoptosis in HL-60 Cells. Apoptosis was one of the important ways that the topo II–targeted drugs kill tumor cells. Accordingly, three methods, flow cytometry analysis after propidium iodide staining with subsequent TUNEL assay and DNA fragmentation analysis, were used to investigate the apoptosis-inducing effects.

Propidium iodide staining for Sub-G_1 content analysis is used to characterize the apoptosis process. Using this assay, we found that R16 and amonafide dose-dependently induced apoptosis (Fig. 5A). Over 40% of HL-60 cells were detected to be apoptotic following the 24-h treatment of R16 at 5 or 10 μmol/L, whereas amonafide at 10 μmol/L drove only about 10% of HL-60 cells to experience apoptosis.

Next, TUNEL assay further showed that R16 at various concentrations ranging from 0.625 to 10 μmol/L for 24 h could obviously trigger HL-60 cell apoptosis. Likewise, those treated with amonafide underwent much less apoptosis (Fig. 5B).

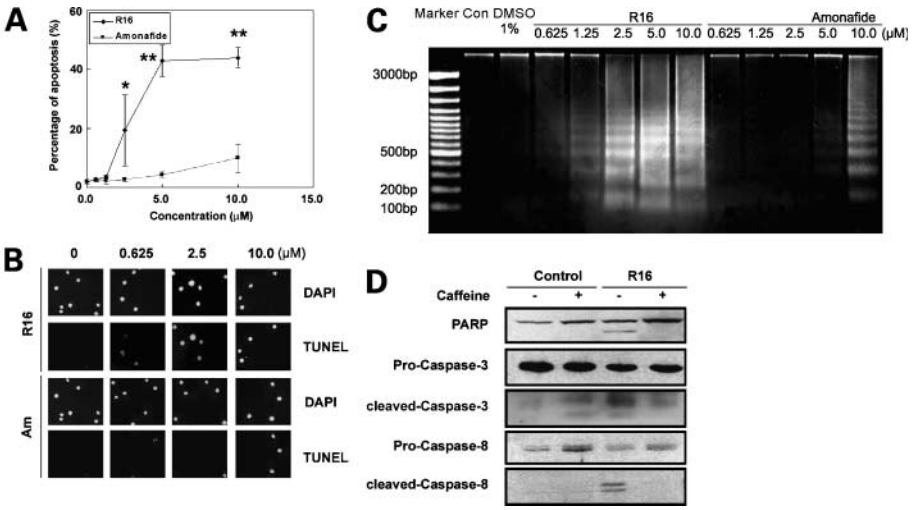

Figure 5. R16-triggered DNA DSBs-mediated apoptosis in HL-60 cells. **A,** percentage of apoptotic HL-60 cells after treatment of R16 or amonafide for 24 h. *Points,* means; *bars,* SD; $n = 3$. The significance of the data was analyzed and indicated. *, $P < 0.05$; **, $P < 0.01$. **B,** DNA fragmentation in HL-60 cells treated with R16 or amonafide for 24 h, as detected by DNA agarose gel electrophoresis. Cells were either left untreated or treated with different concentrations of R16 or amonafide for 24 h. **C,** fluorescent TUNEL labeling of R16- or amonafide-treated apoptotic HL-60 cells. Samples were stained with the TUNEL reaction mixture (Roche), which represented the apoptotic cells and 4′,6-diamidino-2-phenylindole which represented the nucleus of HL-60 cells. **D,** ATM/ATR kinase inhibitor caffeine (2 mmol/L) pretreatment for 1 h abrogated the cleavage of PARP, pro-caspase-3, and pro-caspase-8 induced by R16 (5 μmol/L, 6 h).

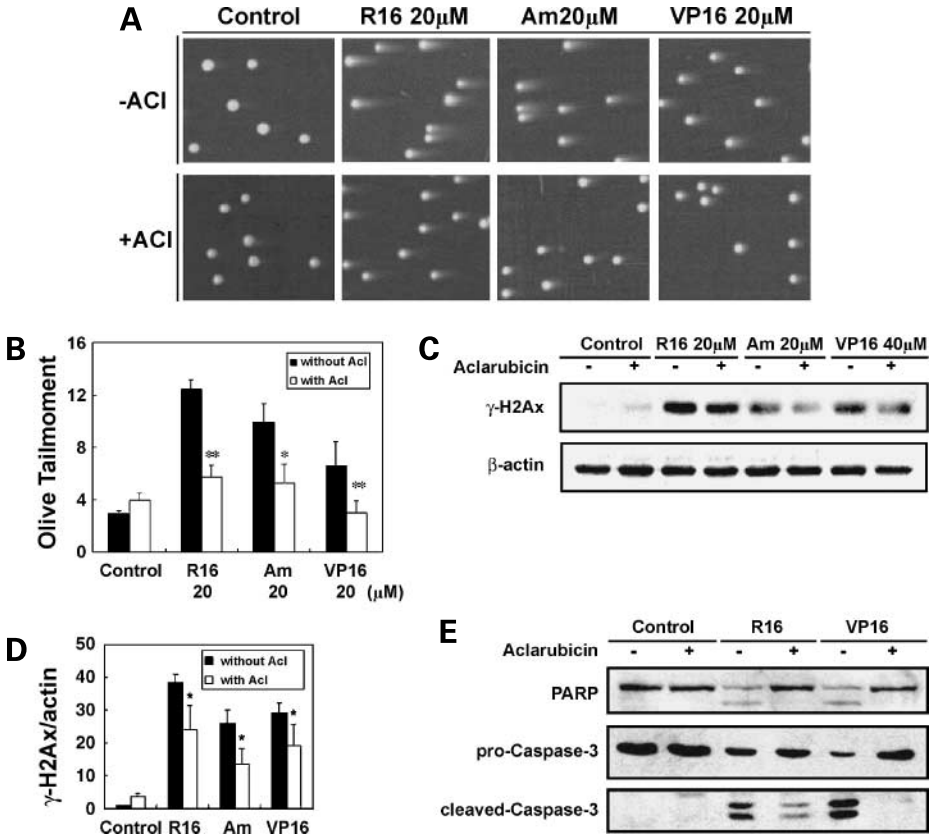

Figure 6. Topo II catalytic inhibitor aclarubicin abated DSBs and apoptosis induced by R16. **A,** HL-60 cells were exposed to R16 (20 μmol/L), amonafide (20 μmol/L), or VP16 (20 μmol/L) for 1 h with or without pretreatment with aclarubicin (50 nmol/L) for 0.5 h. Neutral comet assays were done to evaluate the DSBs. *Row 1*, samples without the preincubation of acalrubicin; *row 2*, samples with the preincubation of aclarubicin. **B,** semiquantitative analyses of the results presented in **A** were expressed as the olive tail moment (mean ± SD, $n = 3$). **C,** aclarubicin abated γ-H2Ax up-regulation in HL-60 cells treated with R16 (20 μmol/L), amonafide (20 μmol/L), or VP16 (40 μmol/L) for 1 h. **D,** semiquantitative densitometry analyses of the results presented in **C** were expressed as relative ratios of γ-H2Ax/β-actin (mean ± SD, $n = 3$). **E,** aclarubicin (50 nmol/L) abrogated the cleavage of PARP and pro-caspase-3 induced by R16 (5 μmol/L, 6 h) or VP16 (5 μmol/L, 6 h).

In addition, we also observed the effects of R16 and amonafide on DNA fragmentation. Results showed that both R16 and amonafide dose-dependently triggered DNA fragmentation. This finding seemed more evident in R16-treated cells than those exposed to amonafide (Fig. 5C).

Caffeine Antagonizes R16-Induced DNA Apoptosis. ATM/ATR kinase inhibitor caffeine was used to examine whether R16-induced apoptosis was caused by DNA DSBs. Thirty minutes pretreatment of caffeine at 2 mmol/L significantly abated PARP cleavage and the activation of both pro-caspase-3 and pro-caspase-8, which were induced by the exposure of R16 at 5 μmol/L for 6 h (Fig. 5D). All these indicate that ATM and/or ATR sensed DNA DSBs probably via the R16-activated apoptosis pathway.

Topo II Cleavage Complexes Drive R16-Induced DNA DSBs and Apoptosis

Topo II poisons are not always capable of inducing apoptosis in a topo II–dependent mechanism. Sometimes, they activate apoptosis cascades bypassing the formation of topo II cleavage complexes. This prompted us to investigate whether the formation of topo II cleavage complexes contributes to R16-mediated apoptosis.

R16-Induced DNA Damage and Apoptosis Are Antagonized by a Topo II Inhibitor Aclarubicin. We first introduced a typical catalytic inhibitor alcarubicin to examine whether it overcomes R16-triggered DNA DSBs. Here, the catalytic inhibitors were selected only because they are able to abrogate topo II poison–induced DSBs via disrupting the formation of cleavage complexes. According to expectation, R16- or amonafide-induced dose-dependent DNA DSBs in HL-60 cells (Fig. 4A and B) was dramatically abolished by aclarubicin pretreatment (50 nmol/L, 30 min; Fig. 6A and B).

Because DNA DSBs are always accompanied by the elevation of the phosphorylated H2AX (γ-H2AX; ref. 31), we next detected whether R16 increases the level of γ-H2AX. As shown in Fig. 6C and D, R16 significantly enhanced γ-H2AX upon 1 h exposure. By contrast, pretreatment of aclarubicin caused a reversal of such an elevation. These findings further help understand the responsive role of aclarubicin in antagonizing R16 and amonafide-induced DSBs.

To understand whether R16- or amonafide-trapped complexes lead to the activation of apoptosis, we preincubated HL-60 cells with aclarubicin (50 nmol/L) for 30 min and then concurrently treated with R16, amonafide, or VP16 for the next 6 h. Aclarubicin pretreatment abated the cleavage of PARP and pro-caspase-3 in R16- or VP16-treated HL-60 cells (Fig. 6E), indicating that topo II accounts for R16- or VP16-induced apoptosis.

R16-Induced Damage, Apoptosis, and Cytotoxicity Are Reduced in Topo II–Deficient Cells. To further confirm that the formation of topo II cleavage complexes is crucial for R16-induced apoptosis, we did the subsequent experiment using topo II–deficient HL-60/MX2 cells. These cell lines are deficient in topo II, with a lowered nuclear

topo IIα content (about 2-fold reduction) and an absence of topo IIβ, and exhibit resistance to mitoxantrone and cross-resistance to VP16, VM-26, and other topo II inhibitors (32). At first, the IC_{50} values of R16, amonafide, several validated topo II poisons, and camptothecin (a topo I poison) were measured in both HL-60 and HL-60/MX2 sublines. Results (Fig. 7A) showed that the RF values of R16 and amonafide were 13.12 and 7.94, respectively, which were quite similar to those of the validated topo II poisons mitoxantrone (59.27), VP16 (40.93), and Adriamycin (8.49). However, there was no significant difference in the IC_{50} values of camptothecin between HL-60 and HL-60/MX2 (Fig. 7A). As expected, both R16 and amonafide exhibited markedly less cytotoxicity against HL-60/MX2 cells. All these findings further favor the important role of topo II in the process of killing HL-60 cells.

In addition, we also found that γ-H2AX was not elevated in all the compound-treated HL-60/MX2 cells, with the exception of camptothecin, which triggered a significant increase of the γ-H2AX (Fig. 7B).

Furthermore, PARP cleavage in both cell lines was evaluated upon the treatment of these compounds (Fig. 7C). Unlike camptothecin, R16, amonafide, mitoxantrone, and VP16 only triggered PARP cleavage in the parent cells but not in HL-60/MX2 cells, further supporting the theory that topo II was indispensable for the R16-, amonafide-, mitoxantrone- and VP16-induced apoptosis. Taken together, these results indicate that the topo II cleavage complex may contribute to R16-induced DNA DSBs, apoptosis, and cytotoxicity.

R16 Triggers Apoptosis in a Caspase-Dependent Pathway

Chemotherapeutic agents, including topo II poisons, induce apoptosis in most cells via two major pathways: death receptor-mediated pathway and mitochondria-mediated pathway (33, 34). The aforementioned result indicated that R16-induced DNA damage–mediated apoptosis is topo II dependent. We are thus interested in addressing how R16 is involved in the activation of apoptosis.

We first investigated the effect of R16 on PARP (a major substrate of caspases) and pro-caspase-3 (an effector caspase). Results showed that R16, at a concentration of 2.5 μmol/L, caused almost a complete cleavage of PARP and pro-caspase-3 in the cells, denoting the caspases' involvement in R16-triggered apoptosis (Fig. 8A). We then evaluated the effect of R16 on the ratio of Bcl-xL/Bax, which plays important roles in the onset of apoptosis (35). R16 significantly down-regulated this ratio (decreased from 1 to 0.27 at a dose of 5 μmol/L), which was accompanied by a subsequent activation of caspase-9 (Fig. 8A) and evident release of cytochrome *c* and AIF (Fig. 8B). All these findings implicated that the mitochondrial pathway involved R16-driven apoptosis (36, 37). We also found that R16 was capable of activating caspase-8 and up-regulating FasL

A

IC_{50} (mean±SD)(μM)	Compounds					
	R16	Amonafide	Mitoxantrone	VP16	ADR	CPT
HL-60	2.04±1.39	8.64±0.95	0.05±0.02	0.77±0.09	0.43±0.18	0.06±0.01
HL-60/MX2	26.71±11.59	68.61±6.85	3.13±0.99	31.51±8.16	3.64±1.03	0.08±0.03
RF	13.12	7.94	59.27	40.93	8.49	1.31
P	0.02*	0.004**	0.008**	0.02*	0.002**	0.31

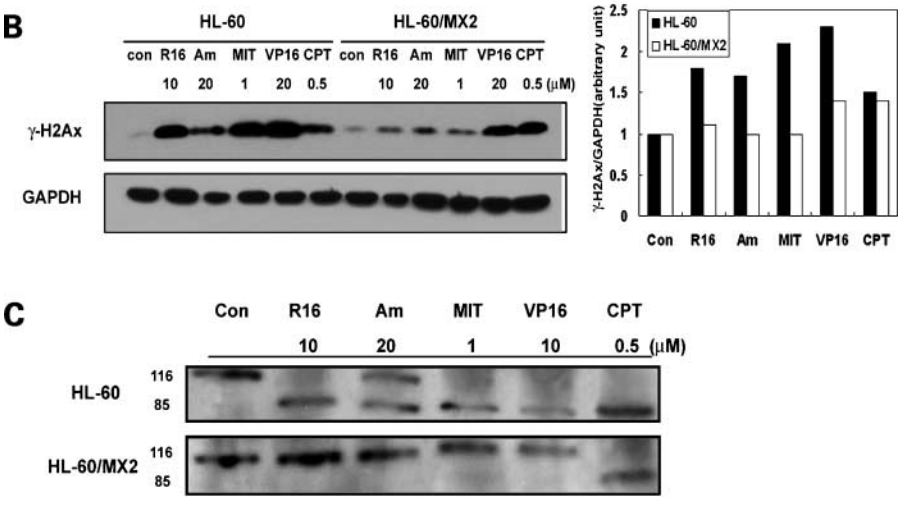

Figure 7. R16 failed to trigger DSBs apoptosis in HL-60/MX2 subline, which was resistant to R16. **A,** Topo II–deficient subline HL-60/MX2 was resistant to R16. Histogram of resistance factors comparison of R16, mitoxantrone, VP16, Adriamycin, and camptothecin (topo I poison, negative reference compound) in HL-60 and HL-60/MX2 was shown. Three separate experiments were carried out to determine the values of IC_{50}, which is expressed as mean ± SD (μmol/L), and the inhibition rates of each concentration of compounds were tested in triplicate. The RF value was calculated as the ratio of the IC_{50} value of HL-60 cells and topo II–deficient HL-60/MX2 cells. **B,** γ-H2Ax up-regulation in the HL-60/MX2 induced by R16, amonafide, and conventional topo II poisons was not as obvious as that in its topo II poison–sensitive parental cells. *Right,* the ratios of γ-H2Ax/glyceraldehyde-3-phosphate dehydrogenase. **C,** PARP cleavage triggered by R16, amonafide, and conventional topo II poisons did not exist in HL-60/MX2 cells. *Top,* the concentrations of compounds.

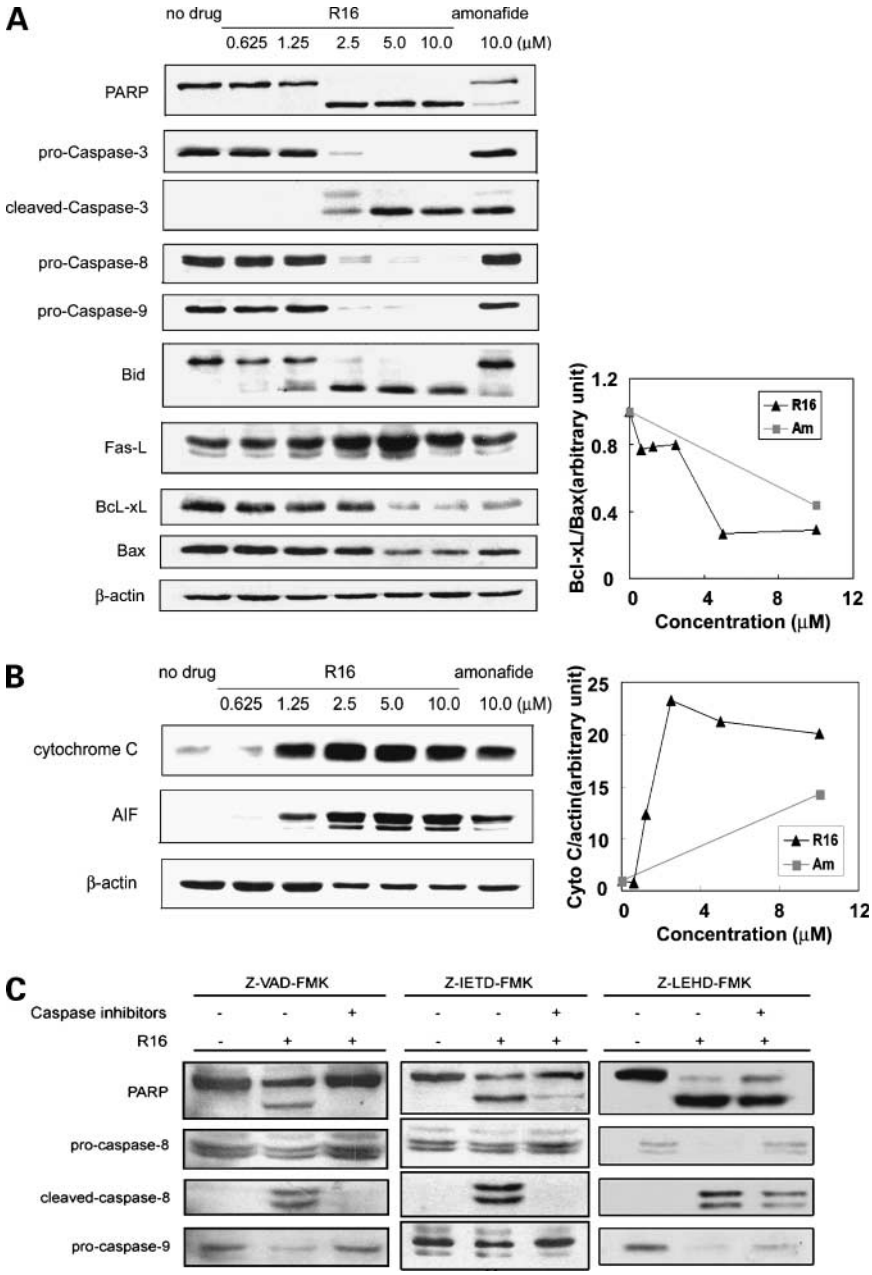

Figure 8. Apoptosis induced by R16 and amonafide is caspase-3, caspase-8, and caspase-9 dependent. **A,** R16-induced apoptosis was involved in the cleavage of pro-caspase-3, pro-caspase-8, and pro-caspase-9. HL-60 cells were cultured with medium or serial diluted concentrations of R16 or 10 μmol/L amonafide for 24 h. PARP, pro-caspase-3, pro-caspase-8, pro-caspase-9, and Bid cleavages were tested, and the expression of Fas-L, Bcl-xL, and Bax was evaluated. *Top,* the concentration of R16 or amonafide. *Right,* the ratios of BCl-xL/Bax. **B,** cytochrome *c* and AIF released from mitochondria. HL-60 cells were treated with or without R16 or amonafide for 24 h, and the separation of mitochondria and cytosol was accomplished. The cytosol samples were analyzed, and the release of cytochrome *c* as well as AIF was evaluated. *Right,* the ratios of cytochrome *c*/β-actin. **C,** pan-caspase inhibitor Z-VAD-FMK, caspase-8 inhibitor Z-IETD-FMK, and caspase-9 inhibitor Z-LEHD-FMK blocked R16-induced cleavage of PARP. HL-60 cells were exposed to R16, 5 μmol/L for 6 h with or without pretreatment with 100 μmol/L Z-VAD-FMK or 25 μmol/L Z-IETD-FMK or 25 μmol/L Z-LEHD-FMK for 30 min.

(Fig. 8A), which alternatively implied the participation of the death receptor pathway in R16-mediated apoptosis (33). Furthermore, the effect of R16 on the cleavage of the Bcl-2 family member Bid (a substrate of caspase-8) to its truncated form (tBid) was investigated, and the latter is an active fragment that interacted with Bax and facilitated cytochrome *c* release (38). Results indicated that the shift toward tBid was significantly elevated following the treatment of R16 (Fig. 8A). This, in turn, favors another story; that R16 senses the intersection of both death receptor-mediated and mitochondria-associated pathways.

To examine whether the inhibition of caspase cleavage abated R16-induced apoptosis, we then evaluated PARP cleavage in 6-h cultures of HL-60 cells with R16 at the dose of 5 μmol/L in the presence or absence of the caspase inhibitors, such as Z-VAD-FMK (100 μmol/L), Z-IETD-FMK (25 μmol/L), and Z-LEHD-FMK (25 μmol/L). As shown in Fig. 8C, pan-caspase inhibitor Z-VAD-FMK completely abolished pro-caspase-8 and pro-caspase-9 cleavage and inhibited PARP cleavage triggered by R16; caspase-8 inhibitor Z-IETD-FMK also blocked the cleavage of PARP and pro-caspase-8; but caspase-9 inhibitor Z-LEHD-FMK was not sufficient to completely abate the PARP and pro-caspase-8 cleavage. These findings alternatively help understand the sequential activation of both caspase-8 and caspase-9, which shows that caspase-8 acts,

at least in part, upstream of caspase-9. The aforementioned appearance of tBid driven by R16 is in further support of this notion.

Discussion

In this study, a novel 5′-substituted amonafide analogue R16 was designed aiming at improving the antitumor efficiency and in particular alleviate the toxicity of the parent compound amonafide. Compared with amonafide, the 5′-substitution is capable of avoiding the metabolite intermediate responsible for the unpredictable side effects. Encouragingly, no possible *N*-acetyl-metabolite was detected in R16-treated mice urine samples using thermospray liquid chromatography–mass spectrometry.[5] In addition, our primary toxicity studies showed that 200 mg/kg amonafide was lethal to mouse, whereas 1.0 g/kg R16-treated mouse survived,[5] indicating a reduced toxicity of R16 *in vivo*. In fact, this chemical manipulation preferentially endowed R16 with less toxicity, better topo II–inhibition ability, stronger apoptosis-induction capacity, and improved antitumor efficiency both *in vitro* and *in vivo*.

Previous evidences of the impact of amonafide or other naphthalimides derivatives on topo II were only restricted to the yeast cells (39) or the cell-free system (8). Given the understanding of the precise mechanisms involved in the antitumor activities of R16 in particular and the naphthalimides compounds in general should aid in rational designing of novel topo II–targeted drugs, it is thus necessary to unravel how R16 targets topo II. In this study, except for molecular evidences from kDNA decatenation assay and topo IIα ATPase domain binding assay (Fig. 3A and D), the performance of the TARDIS assay (Fig. 3B and C) additionally help clarify the indispensable role of R16 in the formation of topo II cleavage complexes functioning as a topo II poison.

Topo II–targeted agents generally result in a series of biochemical changes that culminate in cell death (40). However, the stabilization of covalent topo cleavage complexes is not always sufficient to insure cell death. For example, although topo II poison amsacrine stabilized the equal numbers of topo II cleavage complexes in both control and dinitrophenol-treated L1210 cells, it produced less cytotoxicity in dinitrophenol-treated cells (41). It is thus likely to deduce that the stabilization of topo II cleavage complexes is critical for the fate of the drug-treated cells. Interestingly, this notion stands in contrast to the data on another topo II poison Adriamycin in which Adriamycin-DNA adducts alternatively drove apoptosis in topo II–deficient cells. This separate apoptosis-activated mechanism in such a non–topo II–dependent manner highlighted that the topo II poisons–activated apoptosis can also bypass the formation of topo II cleavage complexes (42). In our study, pretreatment of topo II catalytic inhibitor aclarubicin distinctly abrogated the DNA DSBs and caspases activation in R16-treated cells. In particular, the DNA DSBs induction, apoptosis activation, and cell-killing ability of R16 were evidently reduced in HL-60/MX2 cells (Fig. 7). Based on these findings, we are thus encouraged to disclose that the R16-mediated stable topo II–cleavable complexes dominates its DNA DSBs, apoptosis, and subsequent cytotoxicity.

ATM/ATR, members of the phoshpoinositide kinases–related protein family, are two most important kinases responding to DNA DSBs and subsequent cell cycle arrest and apoptosis (43, 44). It was reported that caffeine, an ATM/ATR kinase inhibitor, could abrogate the DNA damage–induced cell cycle arrest and sensitize the p53-defective cancer cells to DNA damage (45, 46). However, it is not always the case for the topo II poisons upon the introduction to caffeine. Their ability to sensitize cancer cells in the presence of caffeine was subtle and sometimes even more resistant to, in particular, DNA damages (47). In current study, caffeine was capable of counteracting R16-mediated G_2-M arrest and apoptosis (Figs. 4E and 5D), but seemed to be less effective on VP16-triggered apoptosis (data not shown). It was thus likely to conclude that ATM/ATR was deeply involved in R16-induced apoptosis but not VP16-triggered events.

We have shown for the first time that R16 targets topo II by trapping cleavage complexes, which drives DNA DSBs, activates ATM/ATR, and leads to cell cycle arrest and/or apoptosis. The consequently appreciable pharmacologic profiles of R16, including well-defined antitumor activities, anti-MDR capacities, and less toxicity, are attributed to the delicate substitution at the 5-position with a favorable thiol manipulation. This superiority to the parent compound amonafide favors R16, a promising anticancer drug candidate deserving of further development.

Acknowledgments

We thank Li-Juan Lu and Yong Xi for technical assistance in mouse xenograft experiments.

References

1. Wang JC. Cellular roles of DNA topoisomerases: a molecular perspective. Nat Rev Mol Cell Biol 2002;3:430–40.

2. Liu LF. DNA topoisomerase poisons as antitumor drugs. Annu Rev Biochem 1989;58:351–75.

3. Chen AY, Liu LF. DNA topoisomerases: essential enzymes and lethal targets. Annu Rev Pharmacol Toxicol 1994;34:191–218.

4. Andoh T, Ishida R. Catalytic inhibitors of DNA topoisomerase II. Biochim Biophys Acta 1998;1400:155–71.

5. Brana MF, Ramos A. Naphthalimides as anti-cancer agents: synthesis and biological activity. Curr Med Chem Anti-Canc Agents 2001;1:237–55.

6. Scheithauer W, Dittrich C, Kornek G, et al. Phase II study of amonafide in advanced breast cancer. Breast Cancer Res Treat 1991;20:63–7.

7. Costanza ME, Berry D, Henderson IC, et al. Amonafide: an active agent in the treatment of previously untreated advanced breast cancer—a cancer and leukemia group B study (CALGB 8642). Clin Cancer Res 1995;1:699–704.

8. Hsiang YH, Jiang JB, Liu LF. Topoisomerase II–mediated DNA cleavage by amonafide and its structural analogs. Mol Pharmacol 1989;36:371–6.

9. Ratain MJ, Mick R, Berezin F, et al. Paradoxical relationship between

[5] Unpublished data.

acetylator phenotype and amonafide toxicity. Clin Pharmacol Ther 1991; 50:573 – 9.

10. Ratain MJ, Mick R, Berezin F, et al. Phase I study of amonafide dosing based on acetylator phenotype. Cancer Res 1993;53:2304 – 8.

11. Ratain MJ, Rosner G, Allen SL, et al. Population pharmacodynamic study of amonafide: a Cancer and Leukemia Group B study. J Clin Oncol 1995;13:741 – 7.

12. Ratain MJ, Mick R, Janisch L, et al. Individualized dosing of amonafide based on a pharmacodynamic model incorporating acetylator phenotype and gender. Pharmacogenetics 1996;6:93 – 101.

13. Allen SL, Kolitz JE, Lundberg A, et al. Phase I study of amonafide + cytosine arabinoside (AraC) in patients with poor risk acute myeloid leukemia (AML). ASCO Annual Meeting Proceedings 2005;23:6602.

14. Sami SM, Dorr RT, Alberts DS, Solyom AM, Remers WA. Analogues of amonafide and azonafide with novel ring systems. J Med Chem 2000; 43:3067 – 73.

15. Brana MF, Cacho M, Garcia MA, et al. New analogues of amonafide and elinafide, containing aromatic heterocycles: synthesis, antitumor activity, molecular modeling, and DNA binding properties. J Med Chem 2004;47:1391 – 9.

16. Li Z, Yang Q, Qian X. Novel thiazonaphthalimides as efficient antitumor and DNA photocleaving agents: effects of intercalation, side chains, and substituent groups. Bioorg Med Chem 2005;13:4864 – 70.

17. Qian X, Huang T, Wei D. Interaction of naphthyl heterocycles with DNA: effects of thiono and thio groups. J Chem Soc Perkin Trans II 2000; 715 – 8.

18. Skehan P, Storeng R, Scudiero D, et al. New colorimetric cytotoxicity assay for anticancer-drug screening. J Natl Cancer Inst 1990;82:1107 – 12.

19. Miao ZH, Tang T, Zhang YX, Zhang JS, Ding J. Cytotoxicity, apoptosis induction and downregulation of MDR-1 expression by the anti-topoisomerase II agent, salvicine, in multidrug-resistant tumor cells. Int J Cancer 2003;106:108 – 15.

20. Steinfelder HJ, Quentin I, Ritz V. A fast and sensitive technique to study the kinetics and the concentration dependencies of DNA fragmentation during drug-induced apoptosis. J Pharmacol Toxicol Methods 2000; 43:79 – 84.

21. Singh NP, McCoy MT, Tice RR, Schneider EL. A simple technique for quantitation of low levels of DNA damage in individual cells. Exp Cell Res 1988;175:184 – 91.

22. Lu HR, Zhu H, Huang M, et al. Reactive oxygen species elicit apoptosis by concurrently disrupting topoisomerase II and DNA-dependent protein kinase. Mol Pharmacol 2005;68:983 – 94.

23. Tanabe K, Ikegami Y, Ishida R, Andoh T. Inhibition of topoisomerase II by antitumor agents bis(2,6-dioxopiperazine) derivatives. Cancer Res 1991;51:4903 – 8.

24. Willmore E, Frank AJ, Padget K, Tilby MJ, Austin CA. Etoposide targets topoisomerase IIα and IIβ in leukemic cells: isoform-specific cleavable complexes visualized and quantified *in situ* by a novel immunofluorescence technique. Mol Pharmacol 1998;54:78 – 85.

25. Chaoxin H, Zhili Z, Jingui M, et al. Salvicine functions as a novel topoisomerase II poison by binding to ATP pocket. Mol Pharmacol 2006; 70:1593 – 601.

26. Hu T, Sage H, Hsieh TS. ATPase domain of eukaryotic DNA topoisomerase II. Inhibition of ATPase activity by the anti-cancer drug bisdioxopiperazine and ATP/ADP-induced dimerization. J Biol Chem 2002; 277:5944 – 51.

27. Miura K, Aminova L, Murayama Y. Fusarenon-X – induced apoptosis in HL-60 cells depends on caspase activation and cytochrome *c* release. Toxicology 2002;172:103 – 12.

28. Yang F, Chen Y, Duan W, et al. SH-7, a new synthesized shikonin derivative, exerting its potent antitumor activities as a topoisomerase inhibitor. Int J Cancer 2006;119:1184 – 93.

29. Hsiang YH, Liu LF. Evidence for the reversibility of cellular DNA lesion induced by mammalian topoisomerase II poisons. J Biol Chem 1989;264: 9713 – 5.

30. Sarkaria JN, Busby EC, Tibbetts RS, et al. Inhibition of ATM and ATR kinase activities by the radiosensitizing agent, caffeine. Cancer Res 1999; 59:4375 – 82.

31. Rogakou EP, Pilch DR, Orr AH, Ivanova VS, Bonner WM. DNA double-stranded breaks induce histone H2AX phosphorylation on serine 139. J Biol Chem 1998;273:5858 – 68.

32. Harker WG, Slade DL, Drake FH, Parr RL. Mitoxantrone resistance in HL-60 leukemia cells: reduced nuclear topoisomerase II catalytic activity and drug-induced DNA cleavage in association with reduced expression of the topoisomerase II β isoform. Biochemistry 1991;30: 9953 – 61.

33. Petak I, Houghton JA. Shared pathways: death receptors and cytotoxic drugs in cancer therapy. Pathol Oncol Res 2001;7:95 – 106.

34. Debatin KM, Poncet D, Kroemer G. Chemotherapy: targeting the mitochondrial cell death pathway. Oncogene 2002;21:8786 – 803.

35. Shinoura N, Yoshida Y, Asai A, Kirino T, Hamada H. Relative level of expression of Bax and Bcl-XL determines the cellular fate of apoptosis/necrosis induced by the overexpression of Bax. Oncogene 1999;18:5703 – 13.

36. Kaufmann SH, Earnshaw WC. Induction of apoptosis by cancer chemotherapy. Exp Cell Res 2000;256:42 – 9.

37. Arnoult D, Parone P, Martinou JC, et al. Mitochondrial release of apoptosis-inducing factor occurs downstream of cytochrome *c* release in response to several proapoptotic stimuli. J Cell Biol 2002;159: 923 – 9.

38. Desagher S, Osen-Sand A, Nichols A, et al. Bid-induced conformational change of Bax is responsible for mitochondrial cytochrome *c* release during apoptosis. J Cell Biol 1999;144:891 – 901.

39. Nitiss JL, Zhou J, Rose A, et al. The bis(naphthalimide) DMP-840 causes cytotoxicity by its action against eukaryotic topoisomerase II. Biochemistry 1998;37:3078 – 85.

40. Kaufmann SH. Cell death induced by topoisomerase-targeted drugs: more questions than answers. Biochim Biophys Acta 1998;1400: 195 – 211.

41. Kupfer G, Bodley AL, Liu LF. Involvement of intracellular ATP in cytotoxicity of topoisomerase II-targetting antitumor drugs. NCI Monogr 1987; 37 – 40.

42. Swift LP, Rephaeli A, Nudelman A, Phillips DR, Cutts SM. Doxorubicin-DNA adducts induce a non-topoisomerase II – mediated form of cell death. Cancer Res 2006;66:4863 – 71.

43. Shiloh Y. ATM and ATR: networking cellular responses to DNA damage. Curr Opin Genet Dev 2001;11:71 – 7.

44. Pauklin S, Kristjuhan A, Maimets T, Jaks V. ARF and ATM/ATR cooperate in p53-mediated apoptosis upon oncogenic stress. Biochem Biophys Res Commun 2005;334:386 – 94.

45. Yao SL, Akhtar AJ, McKenna KA, et al. Selective radiosensitization of p53-deficient cells by caffeine-mediated activation of p34cdc2 kinase. Nat Med 1996;2:1140 – 3.

46. Wang Q, Fan S, Eastman A, et al. UCN-01: a potent abrogator of G_2 checkpoint function in cancer cells with disrupted p53. J Natl Cancer Inst 1996;88:956 – 65.

47. Traganos F, Kapuscinski J, Gong J, et al. Caffeine prevents apoptosis and cell cycle effects induced by camptothecin or topotecan in HL-60 cells. Cancer Res 1993;53:4613 – 8.

Molecular Cancer Therapeutics

R16, a novel amonafide analogue, induces apoptosis and G_2-M arrest via poisoning topoisomerase II

Hong Zhu, Min Huang, Fan Yang, et al.

Mol Cancer Ther 2007;6:484-495.